JOURNAL OF SPACECRAFT AND ROCKETS
Vol. 57, No. 2, March–April 2020

Electrostatic Tractor Analysis Using a Measured Flux Model

Joseph A. Hughes* and Hanspeter Schaub†
University of Colorado, Boulder, Colorado 80309

https://doi.org/10.2514/1.A34359

Although spacecraft charging is often thought of as a purely harmful phenomenon, if controlled it can be used as a means of touchless actuation. If a tug spacecraft irradiates a nearby debris object with an electron beam, the tug will charge positively and the debris will charge negatively. This creates an attractive Coulomb force that the tug can use to touchlessly tug the debris object from the geosynchronous orbit into a graveyard orbit. Compared with earlier work this paper uses a more advanced charging model with isotropic fluxes for the calculation of electron and ioninduced yields, and an empirical model of electron and ion fluxes rather than Maxwellian distributions. This new model is used to calculate the attractive force for a variety of tug to debris size ratios, beam currents and voltages, and the inclusion of pulsing the electron beam. The major result of using this new charging model is that it takes more current, and thus power, than was used in prior work to charge a debris object due to the higher yields from isotropic fluxes. The electrostatic tractor concept can still move a range of large, tumbling debris objects to the graveyard orbit in a few months.

Nomenclature

A	=	albedo
a	=	semimajor axis, km
b_1, b_2	=	electron range parameters, Å
C, α	=	electron range parameters
d	=	duty cycle
E	=	energy, eV
F	=	differential flux, $1/(\text{cm}^2 \cdot \text{sr} \cdot \text{s} \cdot \text{eV})$
$H()$	=	heaviside step function
I_b	=	electron backscattering current, A
I_{beam}	=	beam current, A
I_e, I_i	=	electron and ion thermal currents, A
I_{ph}	=	photoelectric current, A
I_{SEE_e}, I_{SEE_i}	=	electron and ion-induced secondary electron emission currents, A
j_{ph}	=	photoelectric flux, $\mu\text{A/m}^2$
K_P	=	planetary K index
kT	=	thermal energy, eV
LE	=	landing energy, eV
LT	=	local time, h
m	=	mass, kg
n	=	mean motion, rad/s
n_E, n_I	=	electron, ion density, $\#/\text{cm}^3$
P	=	power, W
Q_T, Q_D	=	tug and debris charges, C
q_1, q_2	=	electron range parameters
R_T, R_D	=	tug and debris radius, m
R	=	electron range, Å
V_b	=	beam accelerating voltage
Y	=	total yield
$\langle Y \rangle$;	=	mean yield
β, E_M	=	ion secondary electron emission parameters
δ	=	secondary electron emission yield
ϵ_0	=	vacuum permittivity ($\epsilon_0 \approx 8.85418782 \times 10^{-12}$, F/m)
η	=	backscattering yield
ρ	=	tug-to-debris distance, m
ϕ	=	voltage, V

Received 24 July 2018; revision received 4 August 2019; accepted for publication 15 November 2019; published online 20 January 2020.

*Graduate Research Assistant, Department of Aerospace Engineering, Engineering Center Electrical Engineering (ECEE) 275, 431 University of Colorado Boulder (UCB).

†Professor and Glenn L. Murphy Chair of Engineering, Department of Aerospace Engineering, Engineering Center North Tower (ECNT) 321, 431 University of Colorado Boulder (UCB). Member AIAA.

I. Introduction

BECAUSE spacecraft charging can cause mission-ending damage, it is often thought of as a harmful phenomenon that must be prevented or mitigated to ensure mission success. However, if controlled, it can have beneficial effects that enable new and exciting missions. For instance, a number of concepts have been proposed to purposely charge a spacecraft so that it is pushed by the Earth's magnetic field through the Lorentz field to change its orbit without expending fuel [1–3]. Another family of concepts use the Coulomb force between a pair of charged spacecraft rather than the interaction with the Earth's magnetic field to exert touchless forces and torques.

If a servicing vehicle irradiates a passive conducting space object with an electron beam, the servicer charges positive and the passive craft charges negative, resulting in an attractive Coulomb force between them. This force can be used for small orbital corrections in a formation-flying mission with negligible use of propellant [4–7]. If the charge distribution on the passive craft is not evenly distributed about the center of mass, the passive craft will also experience an electrostatic torque [8–10]. The concept has broad applicability with propellant-free formation flying and touchless de-spin before docking or servicing. One special case of this concept is the so-called electrostatic tractor (ET), shown in Fig. 1, where a tug craft pulls a piece of space debris from geosynchronous (GEO) orbit into a graveyard orbit 200–300 km higher than GEO Maxwellian [11,12]. Moving GEO debris from the active geostationary belt is important to prevent satellite collisions, which could easily cause more collisions and destroy every satellite in GEO in what is known as the "Kessler" syndrome [13]. Although much orbital debris research focuses on the low Earth orbit (LEO) regime, Oltrogge and Kelso show that the spatial densities in GEO can be as high as those in LEO [14]. Anderson and Schaub [15,16] determines that, given the imperfect mitigation efforts, the number of near-miss events near gravitational wells will double in 50 years. Multiple studies conclude that mitigation measures must be combined with active debris removal to ensure the long-term safety and usability of the GEO ring [17–20].

This paper analyzes the ET concept with a higher-fidelity charging model than has been used before. The first analysis of the charging aspect of the ET [21] included electron and ion thermal currents using a nominal Maxwellian current model, the photoelectric current, and

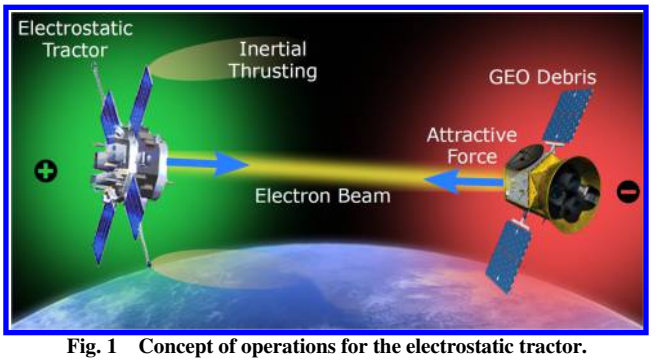

Fig. 1 Concept of operations for the electrostatic tractor.

secondary electron emission (SEE) from the beam electrons, but neglected SEE and backscattering from the thermal currents. Hogan and Schaub in [22] further develop the ET charging model by considering the Maxwellian thermal currents at planetary K-indices of $K_P = 1.5$ and 6. Additionally, they account for SEE and photoelectrons from the debris that provide an additional negative current to the tug. Reference [23] also investigates the performance of the ET with normal variations in the plasma parameters throughout an orbit using single Maxwellian populations based on work by Denton et al. [24]. More force is produced in the early morning sector (local times between 1 and 6) due to the high-temperature electron plasma in that region. Reference [25] investigates a pulsed electron beam with the same Maxwellian-based model as [22] but solve the equations with respect to time to account for the charge-up and discharging behavior. Reference [26] uses the same model as [23] but changes the density and temperature throughout the orbit.

This paper does not use Maxwellian currents at all but rather uses an empirical model [27] to predict the flux as a function of energy, local time (LT), and planetary K index (K_P). The empirical flux distribution is numerically integrated to give the current to the spacecraft as well as the SEE and backscattering yield at a given spacecraft potential. Additionally, all yields, except that from the electron beam, are assumed to be isotropic as opposed to prior work, which used normal incidence. Once the charging model is developed, the ET force is studied for candidate mission scenarios for multiple beam currents and voltages as a function of local time for both a calm space weather condition ($K_P = 2-$) and a stormy space weather condition ($K_P = 8$). Then, the optimal orbit-averaged forces are investigated for many different power and tug-to-debris size levels. Next, pulsing is re-examined for long pulse periods as a function of power and size ratios. All these changes from prior work add fidelity to the charging model, which adds believability to the force and orbital results.

II. Space Environment

In early analysis of charging for the ET, [21–23], electrons were modeled by a single Maxwellian with $n_E \sim 1$ cm^{-3} and $kT_E \sim 1$ keV and ions by a single Maxwellian with $n_I \sim 1$ cm^{-3} and $kT_I \sim 50$ eV. In contrast, the spacecraft charging community often uses much hotter distributions for both ions and electrons with temperatures in the 10 s of keV for electrons and near 30 keV for ions [28]. This work introduces a third model of the GEO space environment.

Denton et al. [27] present an empirical model that uses 82 satellite-years of observed electron and ion flux data. Both populations are measured by magnetospheric plasma analyzers (MPAs) onboard multiple Los Alamos National Labs (LANL) satellites. The MPAs are capable of measuring the flux between 1 eV and 40 keV in three spatial dimensions every 86 s. All of these data are tagged with local time (LT), K_P index, and solar wind electric field (vB_z), which allows interpolation on a variety of cases. The model allows users to specify three inputs (energy, LT, and K_P or vB_z) and outputs the mean, median, and percentile flux values. This work considers a calm case where $K_P = 2-$ and a severe storm with $K_P = 8$. Because the flux is only measured between 1 eV and 40 keV, it is not a complete picture of the environment because there is flux at both higher and lower energies. Also, the measured electron flux at low energies is a combination of the natural space environment and the secondary and photoelectrons generated by the spacecraft itself. Additionally, because the spacecraft is sometimes negative, it will turn away environmental electrons with less energy than the spacecraft's voltage. These two effects both obscure the true environmental electrons below ~100 eV. These contaminations of the electron data and the missing data above 40 keV and below 1 eV are sources of error. For instance, the total density of electrons in the late-night sector at $K_P = 2-$ is slightly less than 1 cm^{-3}, but the ion density is between 2 and 4 cm^{-3}. If this were true, it would seriously violate the principle of quasi-neutrality, which indicates that around 1–3 cm^{-3} of electrons are not counted in this dataset.

To investigate the sensitivity of the following charging analysis to a missing population of electrons, intermediate results were computed with an added Maxwellian population with low density (10^{-5} cm^{-3}) and high temperature (200 keV) [29], as well as a dense (0.1 cm^{-3}) and cold (5 eV) population. The tenuous population makes no significant difference to the charging, but the dense and cold one does reduce the charging.

The statistical mean electron fluxes for GEO are shown in Fig. 2a, with the yellow sheet indicating $K_P = 2-$ and the blue sheet for $K_P = 8$. For the calm condition, the flux monotonically decreases with energy and is fairly smooth with respect to local time. The storm flux is higher nearly everywhere and has a definite hump ~1 keV, and a dramatic trough near local noon. There is also a lot more noisy texture with respect to local time.

The ion fluxes are shown with the same colors indicating the same K_P indices in Fig. 2b. The ion fluxes are more flat with respect to energy than the electron fluxes, but have a more distinct peak at low energy. Once again the storm flux is higher and more textured with respect to local time, although the low energy flux is lower during a storm except for a very sharp peak at local noon.

In the next row of plots, the electron and ion flux is compared to the single and Bi-Maxwellian fits used by NASCAP-2k [28] and shown in Table 1. Figure 2c shows the flux predicted by the three default options for electron flux at GEO alongside two traces from the empirical model—the upper one is chosen as a harsh charging condition ($K_P = 8$, $LT = 6$) and the lower one as a mild condition ($K_P = 2-$, $LT = 18$). The empirical model predicts significantly higher flux at low energies (which may be due to photoelectrons), similar flux at medium energies depending on the K_P and LT, and lower flux at higher energies above 10 keV than the Maxwellian fits.

For aluminum assuming isotropic electron flux, any flux between 120 eV and 6 keV produces more than one secondary electron and contributes to positive charging rather than negative charging. This "positive zone" is grayed out in the plot and sees more flux relative to the high-energy zone above 6 keV in the empirical model than the Maxwellian models, which has implications for the net yields.

The empirical ion flux is compared to the same Maxwellian fits shown in Table 1 and Fig. 2d. The empirical trace solid black line with the large low-energy spike corresponds to $K_P = 8$, $LT = 13$ and the other to $K_P = 2-$, $LT = 2$. The empirical model predicts more flux everywhere than the Maxwellian models, especially at low energies. Additionally, the calm fluxes are much more flat in the empirical model. In the storm condition at local noon, there are two very distinct populations predicted by the empirical model, one with energy near 50 eV, and the other is much more spread out with an energy range of 1–20 keV.

A fundamental property of a Maxwellian fit when plotted on a log-log scale is its shape—it is always a hump with a shallow slope at low energies and steep slope at high energies. Changing the density moves it up and down, and changing the temperature moves it left and right, but neither of these properties change its width. Adding multiple Maxwellian populations with similar energy can approximate a wider peak, but there is no way to produce a narrow peak as is seen in the empirical storm flux at $LT = 13$ using Maxwellian distributions.

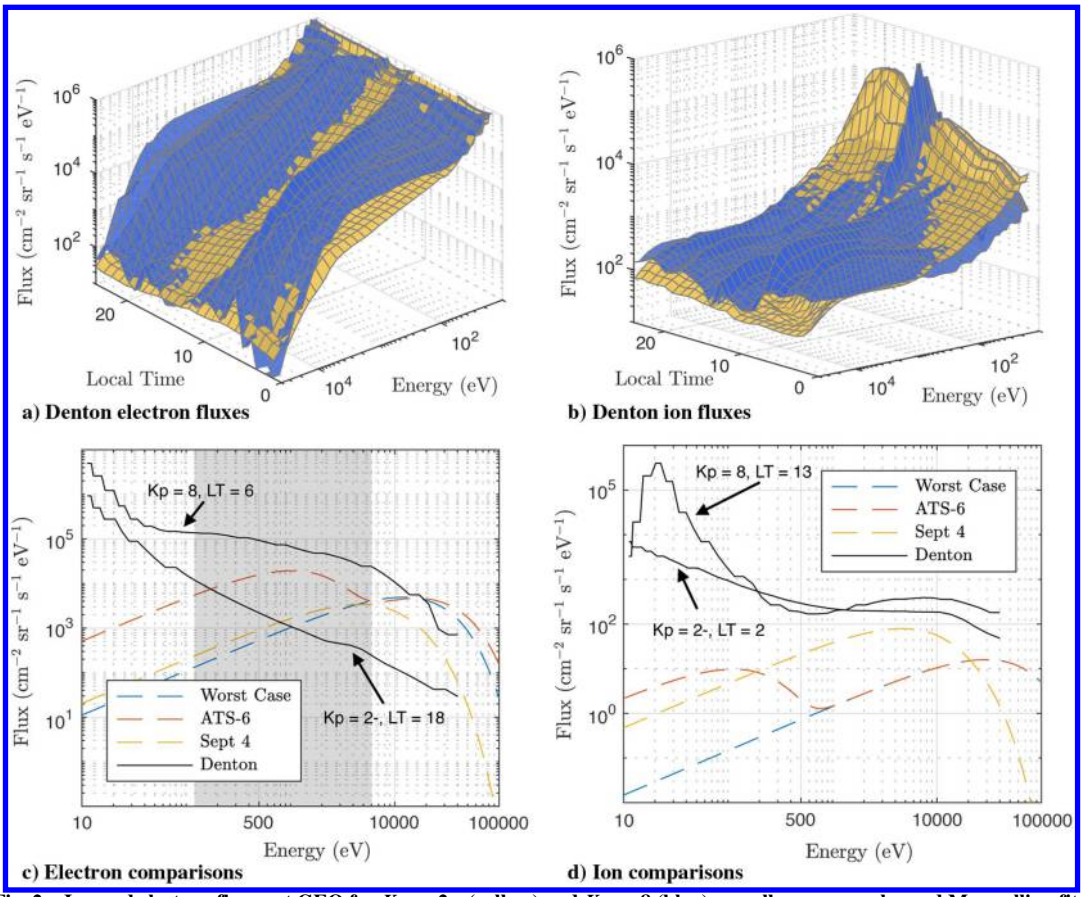

Fig. 2 Ion and electron fluxes at GEO for $K_P = 2-$ (yellow) and $K_P = 8$ (blue) as well as commonly used Maxwellian fits.

Table 1 Space environment fits

	n_E, cm^{-3}	T_E, keV	n_I, cm^{-3}	T_I, keV
NASA worst case	1.1	12	0.24	29.5
ATS-6	1.2, 1.2	16, 1	0.24, 0.00882	29.5, 0.111
Sept. 4	0.3, 0.2	4, 7	0.3, 0.2	4, 7

III. Spacecraft Charging

A space object is subject to many currents from the space plasma and the sun. The currents considered here are the thermal electron and ion currents (I_e, I_i), SEE from both electrons and ions (I_{SEE_e}, I_{SEE_i}), electron backscattering (I_b), the photoelectric current (I_{ph}), and the beam current (I_{beam}). The object is in equilibrium when the net current to it is zero:

$$I_e(\phi) + I_i(\phi) + I_{\text{SEE}_e}(\phi) + I_{\text{SEE}_i}(\phi) + I_b(\phi) + I_{\text{ph}}(\phi) + I_{\text{beam}}(\phi) = 0 \tag{1}$$

The charging model used in this analysis is based on that used in [30]. The main differences are that the beam current is included, the model for electron induced yields is changed to the NASCAP-2k model [31], and all yields other than that from the beam assume isotropic flux rather than normal incidence. This assumes that the beam hits the spacecraft with perfectly normal incidence, not in a grazing impact. Brief explanations for the models for the various currents are presented next.

A. Electron and Ion Thermal Currents

Electrons and ions impact the spacecraft, electrons causing a negative current and ions stealing an electron and causing a positive current. For a flux distribution over energy $F(E)$, the current is [31,32]

$$I(\phi) = q_0 2\pi A \int_L^\infty \left(\frac{E}{E \pm \phi}\right) F(E \pm \phi)\, \mathrm{d}E \tag{2}$$

where q_0 is the particle charge, A is the area exposed to the plasma, and ϕ once again is the spacecraft potential. The lower bound of the integral L is 0 for the repelled particle, and $|\phi|$ for the attracted particle. Ions take the upper sign and electrons take the lower.

Measured flux distributions are used and these integrals are done numerically using an adaptive quadrature integration program that uses linear interpolation on the flux data. The flux data are logarithmically spaced in 40 increments for $K_P = 2-$ and 50 increments for $K_P = 8$ as shown in Figs. 2a and 2b. The lower bound for the attracted particle is $|\phi| + 0.1$ V to avoid a mathematical singularity, and because data for $F(E)$ only exist up to 40 keV for the distributions used, the upper bound is taken as 40,000 V $+ \phi$. Neither the lower bound of 0.1 V nor the upper bound of 40,000 V was found to have a strong impact on the charging results. To counteract some of the enrichment of the low-energy electron flux by photoelectrons and secondary electrons created on the spacecraft, the electron flux at all energies lower than 50 eV is reassigned to the flux at 50 eV.

B. Secondary Electron Emission and Backscattering Current

When an electron or ion impacts a material, it deposits much of its energy in the first few nanometers of the material. Some of this energy goes into freeing electrons near the surface, which can escape the material. This phenomenon is referred to as SEE and can significantly reduce the net electron thermal current and amplify the ion thermal current. Additionally, there is a chance that an electron bounces off the material rather than sticking. This phenomenon is called "backscatter." The probability that an electron will backscatter is given by η, the expected number of secondary electrons generated by a single

incident electron is typically given by δ, and the total yield as $Y = \eta + \delta$. Because the total yield is a function of energy, it must be integrated over the distribution to find the current:

$$I(\phi) = q_0 2\pi A \int_L^\infty Y(E)\left(\frac{E}{E \pm \phi}\right) F(E \pm \phi)\, \mathrm{d}E \tag{3}$$

Rather than calculating the actual current, the mean yield $\langle Y \rangle$ is typically used, which is the effective yield for a particular distribution.

$$\langle Y \rangle = \frac{I_Y}{I} = \frac{\int_L^\infty Y(E)(E/E \pm \phi) F(E \pm \phi)\, \mathrm{d}E}{F \int_L^\infty (E/E \pm \phi) F(E \pm \phi)\, \mathrm{d}E} \tag{4}$$

The mean yield is a function of the distribution (which is a function of LT) and the spacecraft voltage ϕ (which shifts the distribution). Once again, this integral is done numerically using the same adaptive quadrature integration program. The SEE function δ for both ion and electron impact as well as the backscattering function η are discussed next.

The electron-induced SEE yield is typically small at low landing energies, then it rises to a large value for intermediate energies around a few hundred eV, and then falls back to a small yield for keV energies. The NASCAP-2k model [31] for electron-generated SEE as a function of landing energy (E) and angle (ψ) is used with $\psi = 0°$ for the electron beam and a modification [33] to account for isotropic flux (δ_I) for the environmental currents:

$$\delta(E, \psi) = C \frac{1 - e^{-R\alpha \cos(\psi)} \sec(\psi)}{\alpha(b_1 q_1 E^{q_1 - 1} + b_2 q_2 E^{q_2 - 1})} \tag{5}$$

$$\delta_I(E) = 2CE \frac{R\alpha - 1 + e^{-R\alpha}}{(R\alpha)^2} \tag{6}$$

where $R = b_1 E^{q_1} + b_2 E^{q_2}$ is the range of the electrons in the material. For aluminum $b_1 = 154$ Å, $b_2 = 220$ Å, $q_1 = 0.8$, and $q_2 = 1.76$, assuming that the landing energy E is in keV. The parameters C and α are hand-tuned to $C = 9.9808$ and $\alpha = 3.0486e8$ in order to match the peak yield and energy (for incident flux) of 0.97 and 400 eV.

C. Electron Backscattering

Backscattering occurs when an electron is reflected from the spacecraft rather than absorbed. This analysis uses the model for energy-dependent backscattering provided in [31]. First the albedo for normal (A_N) and isotropic (A_I) flux are calculated:

$$A_N = 1 - (2/e)^{0.037Z} \tag{7}$$

$$A_I = 2 \frac{1 - \eta_0(1 - \log(\eta_0))}{\log(\eta_0)^2} \tag{8}$$

and then either are multiplied by a string of Heaviside step functions that account for low energy cases:

$$\eta(E) = \left(\frac{H(1 - E)H(E - 0.05)\log(E/0.05)}{\log(20)} + H(E - 1)\right) \times \left(\frac{e^{-E/5}}{10} + A\right) \tag{9}$$

where E is the landing energy in keV, $H(x)$ is the Heaviside step function, log is the logarithm with base 10, and Z is the atomic number of the material (aluminum in this analysis). The formulas above can be added to produce the total yield $Y(E) = \eta(E) + \delta(E)$ for monoenergetic electrons.

Putting all of this together, the mean yield $\langle Y \rangle$ is shown in Fig. 3 as a function of local time using the empirical model for flux as well as the three chosen Maxwellian fits for a spacecraft at 0 V.

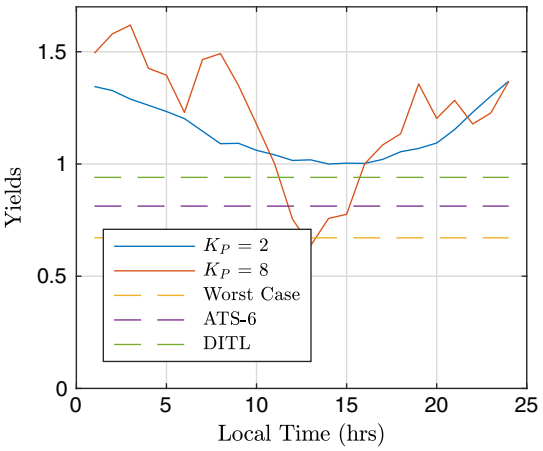

Fig. 3 Mean yields to an uncharged spacecraft using various environmental models.

The yields computed using Denton's model for flux are much higher than those from the Maxwellian distributions—this is due to the difference in flux in the "positive zone" from 120 eV and 6 keV. As a function of local time, the yield in both storm conditions dips near local noon, with it for $K_P = 8$ actually dropping below 1 for a few hours. In all other conditions, the yield is larger than one, which means that the net electron current is positive, and no charging can occur.

In Ref. [34], Ferguson et al. propose that flux above 9 keV is the best proxy for charging, adding that charging will often occur if there is more than 4e8 electrons/cm^2/s above 9 keV. The empirical model predicts flux higher than this threshold when $K_P = 8$ at local times of 6 and 22 (12e8 and 11e8 electrons/cm^2/s of flux, respectively), but the isotropic aluminum yields for both of these instances are above 1, which prohibits any charging. This disagreement between the two models could be for many reasons. It is possible that averaging the flux misses some subtleties that affect the charging. For instance, a very hot but tenuous population one day and a very dense but cold population the next day will average to a flatter population and predict no charging on average, even though on the first day there would definitely have been charging.

Ions may also cause SEE, and for many materials the number of secondaries caused by ions is much larger than that caused by electrons. In this analysis the two parameter Nascap-2k model [31] for isotropic flux is used:

$$\delta(E) = 2 \frac{\beta E^{1/2}}{1 + E/E_M} \tag{10}$$

where E is the energy in keV, and for aluminum $\beta = 1.36$ and $E_M = 40$ are fitting parameters. To get the mean yield, this function must be integrated alongside the ion flux as shown in Eq. (4).

D. Photoelectric Current

Energy from the sun can energize electrons in the first few nanometers of the spacecraft, and so they leave the surface. The fraction that has enough energy to escape the potential well of the spacecraft causes a net positive current given by [35]:

$$I_p = \begin{cases} j_{\mathrm{ph}} A e^{-q\phi/kT_{\mathrm{ph}}} & \phi > 0 \\ j_{\mathrm{ph}} A & \phi \le 0 \end{cases} \tag{11}$$

where j_{ph} is the photoelectron flux, A is the cross-sectional area, and kT_{ph} is the thermal energy of the ejected photoelectrons. For aluminum, $kT_{\mathrm{ph}} = 2$ eV and $j_{\mathrm{ph}} = 40\ \mu\mathrm{A/m}^2$. For a negative spacecraft this current is not a function of voltage, and for a positive spacecraft it quickly vanishes.

E. Beam Current

The electron beam will only escape the potential well of the tug and cause any charging if it has sufficient energy. If it has enough energy to escape the well of the tug, but not to reach the debris, it will deflect and fly off into space and cause a net current on the tug but not the debris. Finally, if the beam is energetic enough it will reach the debris and cause a negative current. The yield for the electron beam is calculated assuming normal incidence and from the landing energy $LE = q_0(V_b - \phi_T + \phi_D)$, where V_b is the accelerating voltage of the beam, and ϕ_T and ϕ_D are the potentials of the tug and debris, respectively. In reality, the debris may be rotating, and so the angle of incidence will change as the angle between the beam and the debris surface changes, which will reduce the effectiveness of the beam.

F. Equilibrium Voltage

For the spacecraft to be in equilibrium with its environment, it must assume the voltage that causes no net current. Voltage and potential are relative quantities, but here we use the voltage with respect to infinity so that we can compute the charges. This is done numerically by root solving Eq. (1) for different local times and different net beam current densities. The beam current density is computed as the actual beam current (which would be directed in a small spot) divided by the total surface area of the spacecraft. For the debris, this current must be reduced using the yield. The photoelectric current is only applied on $1/4$ of the total surface area, because the cross-sectional area of a sphere is $1/4$ the total area. This normalization allows the spacecraft charging calculations to be done once and then interpolated to cover a wide variety of cases. These voltages are shown in Fig. 4.

The top plot of Fig. 4a shows the equilibrium voltage at $K_P = 2-$ computed using the empirical model. The upper sheet represents the tug for which the beam is a positive net current, and the lower sheet represents the debris for which the beam is negative. The limits for the top two plots are -100 to 100 kV to allow for comparison. The most obvious trend is that it takes less beam current to charge negative than positive. Next, at low beam currents it is very hard to charge negative. This is because the photoelectron current very effectively resists any negative charging until it is overwhelmed by the beam. It is easiest for the tug to charge positive in the late night sector, and easiest for the debris to charge negative near local midnight.

The middle plot of Fig. 4b shows the tug and debris equilibrium voltages in the same format, but for $K_P = 8$. There is a lot more variation over local time during a storm—the tug can charge positive very easily near local noon and has a difficult time everywhere else. The debris has a much more complex trend across local time, but it experiences both more and less charging than the calm case at different local times.

The bottom plot of Fig. 4c compares the equilibrium voltage found using the empirical model with that from using the Sept. 4 Bi-Maxwellian fit, a single Maxwellian fit used in prior charging analysis of the ET, and the SCATHA data. The empirical voltages are shown as colored blocks that encompass the curves at all local times, with yellow and blue representing the calm and stormy conditions. The increased variation over local time at $K_P = 8$ can clearly be seen in this format. The Sept. 4 model uses the Bi-Maxwellian fit presented in Table 1 and predicts more positive charging than the empirical model at either storm condition at high currents. It also predicts a much more negative voltage for the debris once the current overpowers the photoelectron current ($10\ \mu\text{A/m}^2 = j_{\text{ph}}/4$). This is because the ion populations are very hot, which reduces the ion current significantly. The fit from prior work uses the parameters from Hogan and Schaub [22], and due to the much lower ion temperature it predicts a less extreme voltage for the debris past the photoelectric cutoff. The SCATHA data are taken from [36], where the spacecraft emitted an electron beam and charged itself up to 3 keV. Because the charging was often limited by the energy of the beam, the spacecraft voltage at that beam current might be even higher if the beam energy was increased. The surface area of SCATHA, if approximated by a cylinder, is 13.5 m^2 [37]. SCATHA is made from many different materials with different SEE parameters and is also spinning, which changes the sunlit area as a function of time; thus, these data points are provided more as an order of magnitude estimate.

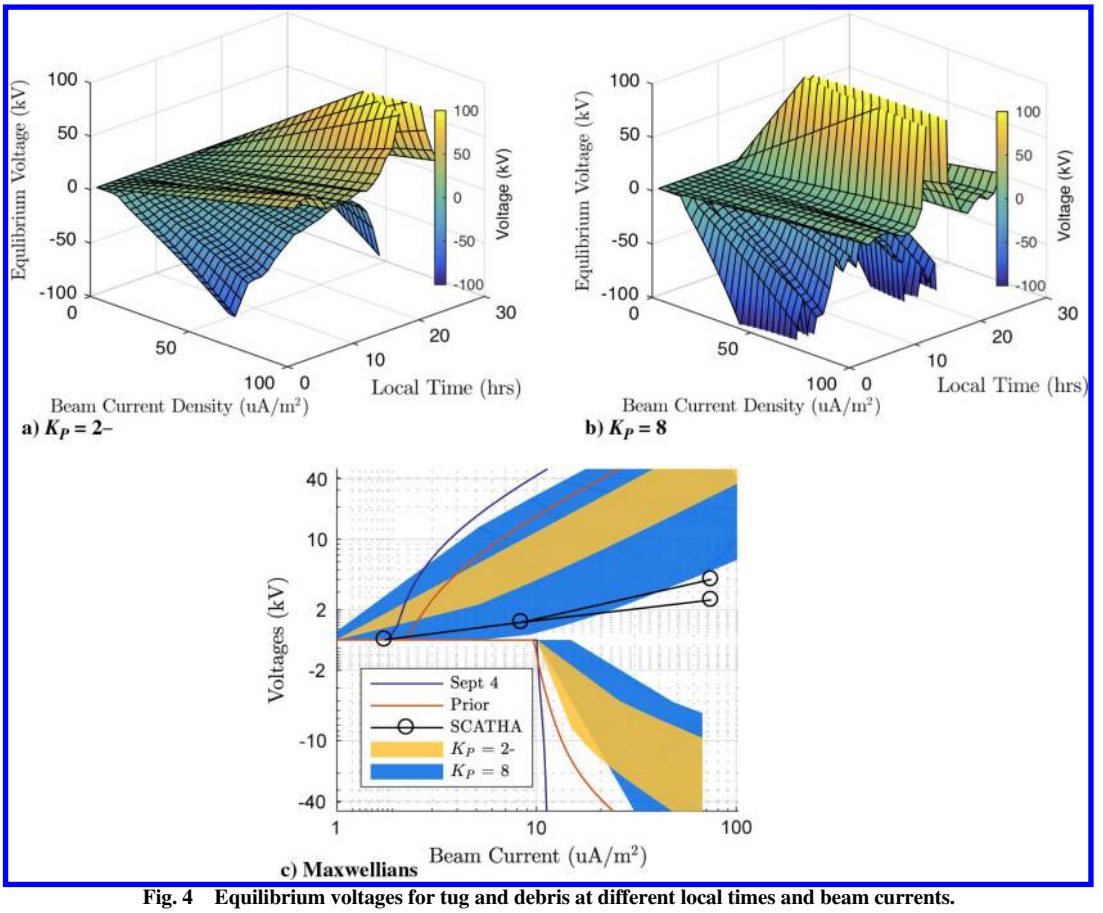

Fig. 4 Equilibrium voltages for tug and debris at different local times and beam currents.

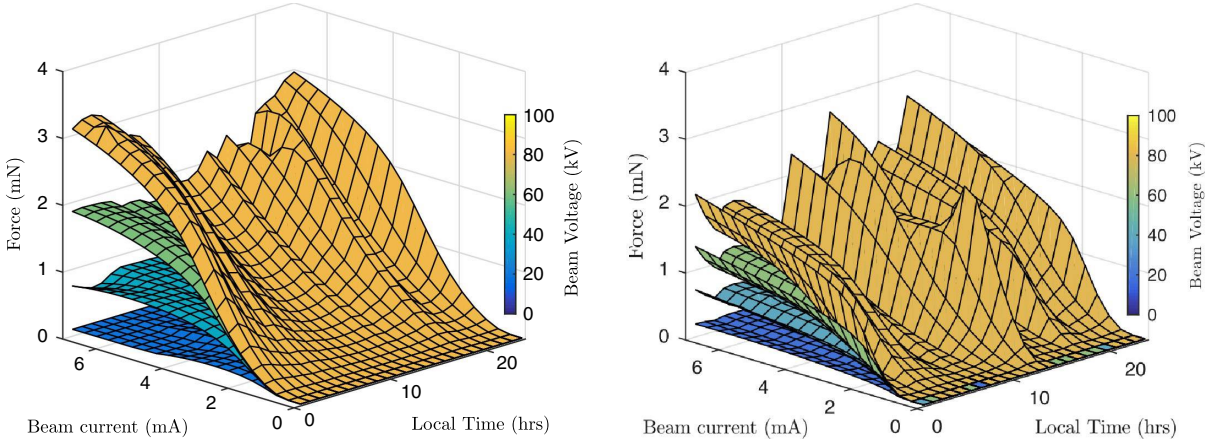

a) $K_P = 2-$ **b)** $K_P = 8$

Fig. 5 Force between a 3 m tug and 2 m debris separated by 20 m as a function of beam current, voltage, and local time.

The charging models based on Maxwellian flux, empirical flux, and the SCATHA data all have sources of error. For the purposes of the ET, which takes a few months to tow a debris object out of GEO, the empirical flux data changing model is used because it provides a better estimate of the average space weather that would be encountered on such a multimonth trip. It is worth noting that all three classes of models predict similar trends in performance.

IV. Force Analysis

To find the force between two spacecraft, the tug and debris radii must be chosen along with the beam current and energy. Using the tug radius and beam current along with local time, the tug potential can be found by directly interpolating the top sheet of Fig. 4. Finding the debris potential is unfortunately more difficult. The yield from the electron beam reduces the net current and is a function of the landing energy of the beam. Thus, to find the net electron beam current and interpolate the debris potential, one would need to already know the debris potential in order to compute the yield. To solve this problem, a function is written that takes a candidate debris voltage and then computes the actual beam current as well as the needed beam current to support that voltage. The debris voltage is varied so that these two numbers are identical. Using this procedure, the equilibrium voltages of two spacecraft can be found easily as a function of their sizes, beam energy and current, and the local time.

Once the voltages (ϕ) are known, they must be transformed to charges to compute the force. The charges are related to the voltages through an elastance matrix:

$$\begin{bmatrix} \phi_T \\ \phi_D \end{bmatrix} = \begin{bmatrix} 1/R_T & 1/\rho \\ 1/\rho & 1/R_D \end{bmatrix} \begin{bmatrix} Q_T \\ Q_D \end{bmatrix} \tag{12}$$

where ρ is the center-to-center distance between the spheres, R_T, R_D are the tug and debris radii, and Q_T, Q_D are the tug and debris charges. Then, the force is computed with Coulomb's force law:

$$F = \frac{Q_T Q_D}{4\pi\epsilon_0 \rho^2} \tag{13}$$

A sheath will form around both spacecraft, which will reduce the force between them, but it is ignored in this analysis. Prior work [38] has shown that the reduction in force is very small, typically less than 1%, for the small separations considered here. However, on rare occasions very dense plasma can make its way into GEO in the afternoon sector [39] and this would introduce significant shielding and make charging much more difficult. The overlapping sheaths from both objects will also change the current balance, but a particle in cell (PIC) simulation is needed to quantify this effect.

Consider the example case of a 3 m tug and a 2 m debris separated by $\rho = 4(R_T + R_D) = 20$ m. The attractive force between them is shown in Fig. 5 at $K_P = 2-$ and $K_P = 8$. The force generally increases with a higher voltage and current and has a decent amount of texture with respect to local time. The highest force is near local midnight for the calm space weather condition when it is easiest for the debris to charge very negative. The force grows quickly with current when the current is low, but seems to saturate at higher currents. During storm time there is a lot more variation in force throughout the orbit, and the force actually decreases with current for some local times.

V. Average Force Analysis

The total re-orbiting time is better related with the orbit-averaged force than the instantaneous force. The orbit-averaged force is computed by averaging the forces across local time. These forces are shown in Fig. 6 for a 20, 40, 60, and 80 kV beam, assuming the same 3 m tug and 2 m debris separated by 20 m. The continuous lines represent $K_P = 2-$, and the dashed lines represent $K_P = 8$.

The 20 kV beam performs just as well as the higher energy beams until about 1 mA, where the higher-energy beams begin to outperform. The 40 kV beam has similar performance to the higher-voltage beams until about 2 mA, and the 60 kV has similar performance to the 80 kV beam until 3 mA. The reason for this behavior is that the extra beam voltage does not increase the force until the debris and tug are charged so differently that the extra accelerating voltage is needed for the beam to reach the debris. These departure currents must be the currents at which the potential difference between the two craft is either 40, 60, or 80 kV. The SEE current is also a function of the landing energy, which is why the curves are not quite identical below the departure currents.

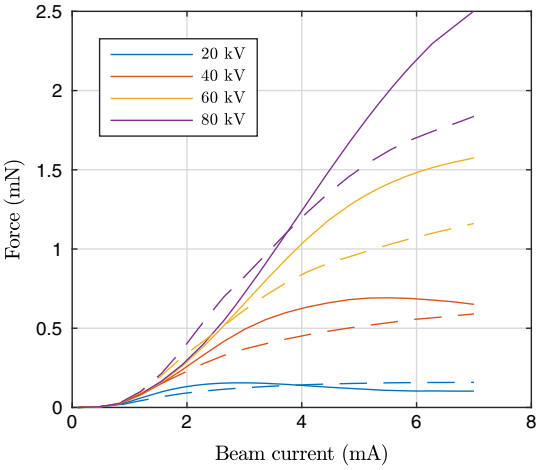

Fig. 6 Orbit averaged force as a function of beam current, voltage, and local time. Dashed lines represent $K_P = 8$, and continuous lines represent $K_P = 2-$.

The orbit averaged storm forces are slightly lower than the calm forces except for low current for the 80 kV beam and high current for the 20 kV beam. This differs from prior work [22,26], which always found higher forces during a storm. This difference is due to the very different charging and environmental models used, which only share the model for the photoelectric current.

VI. Relative Sizing Analysis

In prior work, Hogan [40] found that small tug vehicles would have a hard time charging a much larger debris object. This is because while the beam current is enough to cause significant charging on the small tug, it will barely overcome the photoelectric current on the large debris. This analysis is repeated here, but from a force rather than charging perspective. Because of the induced charge, there is an attractive force even if there is no change in the debris voltage. The force as a function of beam power between a 3 m tug and different debris sizes is shown in Fig. 7a. The separation distance for all cases is 20 m.

The maximum force is found as a function of power for a variety of different debris sizes—the tug size is fixed at 3 m, and so the ratio of tug to debris radius spans from 0.5 up to almost 2. The force is very linear with power with a slope of roughly half a mN per 100 W of power regardless of debris size. Because it is difficult to see departures from this trend at this scale, the difference in force from this linear fit is shown in Fig. 7b. The highest force (or least negative in this plot) is when $R_D = R_T = 3$ m at most powers with $R_D = 2$ and 4 m very near. The extreme ends of the spectrum where R_D is 1.5 or 5 m produce less force. This is because the beam can be close to optimal for both craft when they are the same size, but not when they are different sizes.

VII. Pulsing Analysis

Prior work has considered a pulsed electron beam rather a constant-current beam [25,26]. The benefits to pulsing are twofold: first it introduces windows where both spacecraft are discharged and the beam is off, which can be used for communications, thrusting, or measurements to be taken that might be interfered with by the beam; second, pulsing the beam can increase the force at a given power level. To motivate this phenomenon consider two electron beams, one with energy of 10 keV continuously operating and one with 20 keV of energy on for half the time. Further assume that the current for both beams is the same so that they have the same average power. The 10 keV beam would charge the tug and debris to 5 keV and −5 keV and hold them there, whereas the pulsed beam could charge the tug and debris to ±10 keV when the beam is on and 0 V when it is off. If mutual capacitance is ignored, the pulsed tug and debris charges will both double the continuous case during the time that the beam is on. Because the force is proportional to the product of the charges, the pulsed case will have 4 times the force when the beam is on and zero when it is off. This amounts to the average pulsed force being double that of its continuous counterpart. Of course, the current must also be raised so that the voltage cannot quite double, and there are a few other effects that limit the force increase.

In this analysis, the optimal force at different power levels shown in Fig. 7 will be reused. If the pulse period is large compared with the charge up time, the force that a pulsed beam produces can be approximated as the equilibrium force for the duration of the pulse period. Because the capacitance of the objects considered here is around $4\pi\epsilon_0 R \approx 10^{-10}$ F, a 1 mA beam could change the voltage by 1 kV in approximately 0.1 ms; this assumption of steady-state forces will be valid for all pulse periods larger than 1 s. Hughes and Schaub [25] numerically integrated the full equations and found charge-up times of a few milliseconds, which supports this assumption.

With this assumption the charge-up and charge-down behavior is ignored, and the average force produced by a pulsed beam is given by

$$F_P(P, d) = dF_M(P/d) \tag{14}$$

where $F_M(x)$ is the maximum force at a power level of x, and F_P is the average force from a pulsed beam at power P with a duty cycle of d, which is the fraction of time that the beam is on. During the "on" part of the cycle, the power can be raised to P/d without changing the average power because it is not operating while the beam is off. Multiplying the force by d accounts for it being on only the fraction d of the time.

If the maximum force is directly proportional to power, there is no benefit at all to pulsing, because the ds would cancel each other out. However, if the force increases quadratically, or is linear with an offset, there can be an increase in force. The increase in force from moving from a continuous beam to a pulsed beam of the same power is shown in Fig. 8 for the case of the tug and debris both having a radius of 3 m.

A pulsed beam almost always increases the force for a given power level, with the largest gains found for low-power and low-duty cycles. For very low powers, the pulsed force can be more than 2 times larger than the continuous force, and even at 100 W a pulsed beam can improve the force by 25%. Because the max beam voltage is set at 100 kV, the low-duty-cycle beams are infeasible at high power levels because they require too high of a beam voltage while the beam is on. The increases are larger during stormy conditions especially near 25 W.

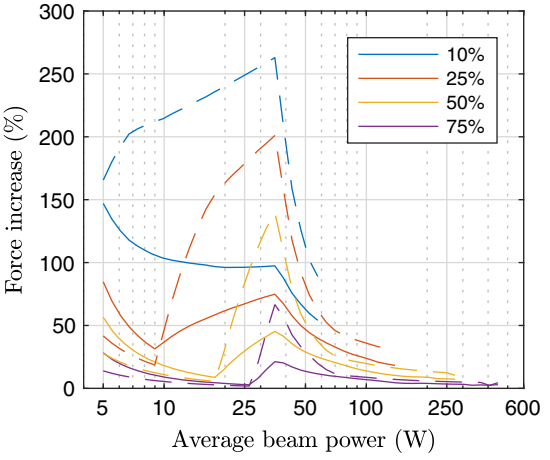

Fig. 8 Force increase as a function of duty cycle and power. Continuous lines represent $K_P = 2-$, and dashed lines represent $K_P = 8$.

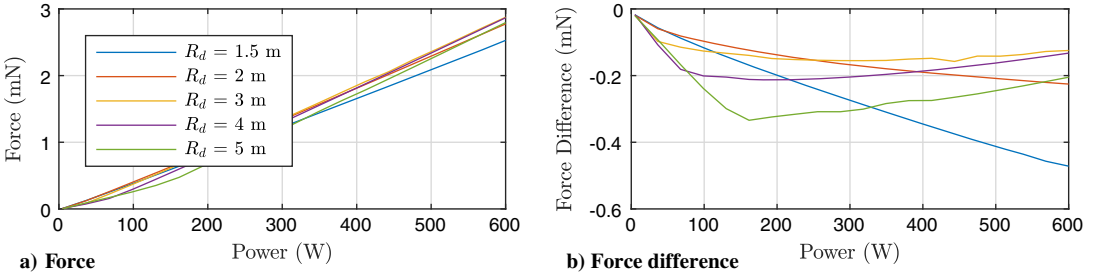

a) Force **b) Force difference**

Fig. 7 Best possible force at different powers for different tug-to-debris size ratios at $K_P = 2-$.

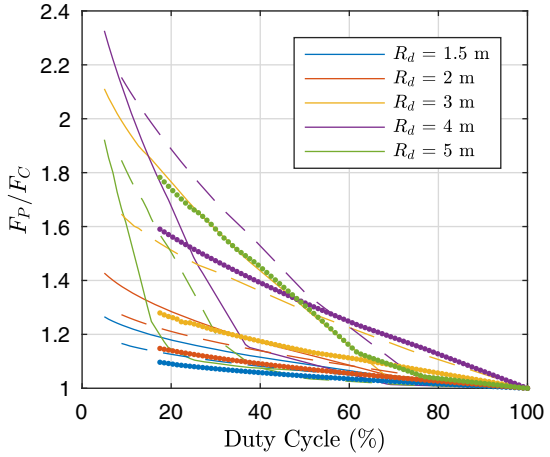

Fig. 9 Force ratio as a function of tug and debris sizes and duty cycle at $K_P = 2-$ with continuous lines representing 25 W, dashed lines representing 50 W, and dots representing 100 W of power.

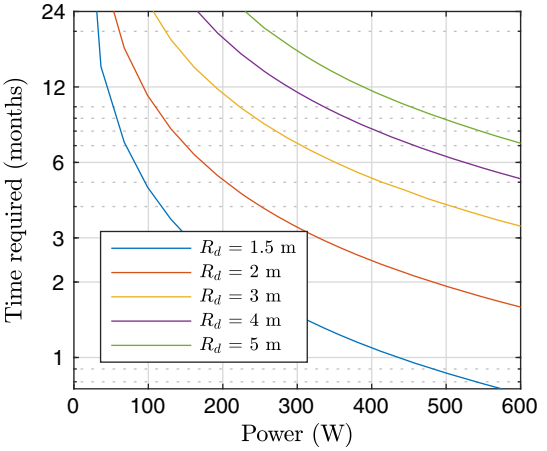

Fig. 10 Time to move GEO debris to a graveyard orbit for a 3 m tug.

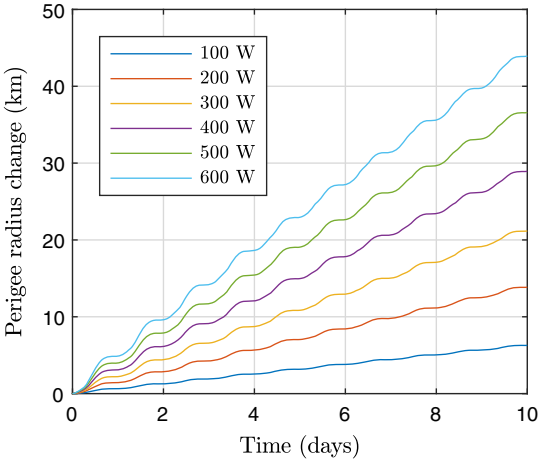

Fig. 11 Change in perigee radius over 1 week of operation.

Now consider varying the tug-to-debris size ratio as well as pulsing. Referring again to Fig. 7, the force is more convex when the debris is larger than the tug. This would indicate that pulsing would be more advantageous when the tug is smaller than the debris because the gain from the force at the higher power level $F_M(P/d)$ would outweigh the loss from only being on d of the time. The ratio of the pulsed to continuous force is shown in Fig. 9.

The force ratio is shown for the power levels of 25 W (continuous lines), 50 W (dashed lines), and 100 W (dots). The lines end at low duty cycles when the beam voltage required is larger than 100 kV, which happens sooner for the high-power cases than the low-power ones. The force ratio is by definition 1 at a 100% duty cycle, and either increases or decreases for different debris sizes. All debris sizes benefit from pulsing at these power levels, but the biggest gains are for the larger debris (green and purple lines). The smallest debris object additionally starts to trend downward for very low duty cycles.

VIII. Orbit Raising

If the forces as a function of local time are used as a purely along-track acceleration in Gauss's variational equations, the change in the orbit can be found. The acceleration is found by estimating the mass from the relationship originally presented in [11] and dividing to find the acceleration.

$$m(kg) = 1507(R(m) - 1.152) \tag{15}$$

First the semimajor axis (SMA) change per orbit equation [11] for a purely along track acceleration is

$$\Delta a = \frac{4\pi}{n^2}\frac{F}{m} \tag{16}$$

where n is the mean motion of the orbit. Then, for each debris radius and power level, calculate the time it would take to raise the SMA by 250 km using the mean motion at its initial orbit radius. This is shown in Fig. 10. In general using more power reduces the time it takes to move the debris to the graveyard orbit, but the gains are greater at lower powers. It takes the 3 m tug a little more than 3 months to tug another 3 m object to the graveyard orbit. In contrast, it only takes 22 days if tugging a 1.5 m debris, and 7 months if tugging a 5 m object. Clearly the ratio between the debris and tug sizes is very important for tugging. Keeping in mind that the tug size is purely for self-capacitance and current collection, with sufficiently large deployable structures, the tug could be a lightweight CubeSat.

Next, consider a higher-fidelity orbital analysis but only for one scenario. The rates of the classical orbit elements are found due to the acceleration, which changes with local time and integrated with an RK4 integrator. The only rates of interest that have a sensitivity to an along-track acceleration are the SMA, the eccentricity, and the argument of perigee.

This analysis can show how long it will take a tractor to pull a debris object into the graveyard orbit, and also what happens to the other orbital parameters during this operation. Consider a 3 m tug and 2 m debris object separated by 20 m at nominal altitude inclined by 1°. The change in the perigee radius is shown in Fig. 11. The perigee radius is shown rather than the SMA because that is the parameter that needs to be increased in order to prevent future collisions.

If the tractor can use 600 W of power, it can tug this debris object into the graveyard orbit in 57 days using this average rate. The beam voltage required is 77 kV and the current is 7.8 mA. If it can use only 100 W of power, it will take 398 days, or 13 months. These estimates predict slightly larger times to the graveyard orbit then Fig. 10, but are still in the same ballpark. This is expected because the analytical method does not account for the changing eccentricity or the coupled nature of the rates.

IX. Conclusions

A new charging model for the ET is developed that uses an empirical model for the electron and ion fluxes, which is used to compute the thermal electron and ion currents as well as the SEE and backscattering yields as well as accounting for isotropic incidence in the yields. The major impact of this new model relative to prior work is that it is much harder for an object to charge negative due to the higher yields. This model is used to predict the forces for a variety of beam currents and voltage as well as tug and debris sizes at both $K_P = 2-$ and $K_P = 8$. It is found that the force is highest near local midnight, and that the orbit averaged forces depend only

on the beam voltage past a current threshold. The forces are mostly linear with power with a slope of around half a mN per 100 W for a 3 m tug.

Pulsing is the most effective for large debris objects at low power, but pulsing still provides force increases for all scenarios evaluated as well as opening windows for controls and sensing to take place without interference from the beam. Orbit raising is considered next; the ET is most effective when tugging small debris, but that is only because they are assumed to be light. A tug spacecraft could also deploy large conducting surfaces to increase its effective radius without significantly changing its mass. For many scenarios, a tug could pull a debris object from the operational GEO ring to a graveyard orbit in a few months. Overall, the higher-fidelity charging model finds that more current and power is required to operate the ET, but it is still a feasible mission concept for touchlessly tugging space debris to the graveyard orbit.

Acknowledgment

This research was funded through Grant FA9550-15-1-0407 from the Air Force Office of Scientific Research.

References

[1] Streetman, B., and Peck, M. A., "New Synchronous Orbits Using the Geomagentic Lorentz Force," *AIAA Journal of Guidance, Control, and Dynamics*, Vol. 30, No. 6, Nov.–Dec. 2007, pp. 1677–1690. https://doi.org/10.2514/1.29080

[2] Streetmann, B., and Peck, M. A., "Gravity-Assist Manuvers Augmented by the Lorentz Force," *Journal of Guidance, Control, and Dynamics*, Vol. 32, No. 5, Oct. 2009, pp. 1639–1650.

[3] Yan, Y., Huang, X., and Yang, Y., *Dynamics and Control of Lorentz-Augmented Spacecraft Relative Motion*, Springer, Singapore, 2017.

[4] Berryman, J., and Schaub, H., "Analytical Charge Analysis for 2- and 3-Craft Coulomb Formations," *AIAA Journal of Guidance, Control, and Dynamics*, Vol. 30, No. 6, Nov.–Dec. 2007, pp. 1701–1710. https://doi.org/10.2514/1.23785

[5] Hogan, E., and Schaub, H., "Collinear Invariant Shapes for Three-Craft Coulomb Formations," *Acta Astronautica*, Vol. 72, March–April 2012, pp. 78–89. https://doi.org/10.1016/j.actaastro.2011.10.020

[6] Jasch, P. D., Hogan, E. A., and Schaub, H., "Out-of-Plane Stability Analysis of Collinear Spinning Three-Craft Coulomb Formations," *Acta Astronautica*, Vol. 88, July–Aug. 2013, pp. 89–97. https://doi.org/10.1016/j.actaastro.2013.03.005

[7] King, L. B., Parker, G. G., Deshmukh, S., and Chong, J.-H., "Study of Interspacecraft Coulomb Forces and Implications for Formation Flying," *AIAA Journal of Propulsion and Power*, Vol. 19, No. 3, May–June 2003, pp. 497–505. https://doi.org/10.2514/2.6133

[8] Bennett, T., Stevenson, D., Hogan, E., McManus, L., and Schaub, H., "Prospects and Challenges of Touchless Debris Despinning Using Electrostatics," *Advances in Space Research*, Vol. 56, No. 3, 2015, pp. 557–568. https://doi.org/10.1016/j.asr.2015.03.037

[9] Bennett, T., and Schaub, H., "Touchless Electrostatic Three-Dimensional Detumbling of Large Axi-Symmetric Debris," *Journal of Astronautical Sciences*, Vol. 62, No. 3, 2015, pp. 233–253. https://doi.org/10.1007/s40295-015-0075-8

[10] Stevenson, D., and Schaub, H., "Terrestrial Testbed for Remote Coulomb Spacecraft Rotation Control," *International Journal of Space Science and Engineering*, Vol. 2, No. 1, May 2013, pp. 96–112.

[11] Schaub, H., and Jasper, L. E. Z., "Orbit Boosting Maneuvers for Two-Craft Coulomb Formations," *AIAA Journal of Guidance, Control, and Dynamics*, Vol. 36, No. 1, Jan.–Feb. 2013, pp. 74–82. https://doi.org/10.2514/1.57479

[12] Schaub, H., and Moorer, D. F., "Geosynchronous Large Debris Reorbiter: Challenges and Prospects," *The Journal of the Astronautical Sciences*, Vol. 59, Nos. 1–2, 2014, pp. 161–176.

[13] Kessler, D. J., and Cour-Palais, B. G., "Collision Frequency of Artificial Satellites: The Creation of a Debris Belt," *Journal of Geophysical Research*, Vol. 83, No. A6, June 1978, pp. 2637–2646. https://doi.org/10.1029/JA083iA06p02637

[14] Oltrogge, D., and Kelso, T., "Getting to Know Our Space Population from the Public Catalog," *Astrodynamics Specialist Conference*, AAS Paper 11-416, Piscataway, NJ, 2011.

[15] Anderson, P. V., and Schaub, H., "Local Orbital Debris Flux Study in the Geostationary Ring," *Advances in Space Research*, Vol. 51, No. 12, 2013, pp. 2195–2206. https://doi.org/10.1016/j.asr.2013.01.019

[16] Anderson, P. V., and Schaub, H., "Local Debris Congestion in the Geosynchronous Environment with Population Augmentation," *Acta Astronautica*, Vol. 94, No. 2, Feb. 2014, pp. 619–628. https://doi.org/10.1016/j.actaastro.2013.08.023

[17] McKnight, D. S., and Pentino, F. R. D., "New Insights on the Orbital Debris Collision Hazard at GEO," *Acta Astronautica*, Vol. 85, April–May 2013, pp. 73–82. https://doi.org/10.1016/j.actaastro.2012.12.006

[18] McKnight, D., "Pay Me Now or Pay Me More Later: Start the Development of Active Orbital Debris Removal Now," *Advanced Maui Optical and Space Surveillance Technologies Conference*, Sept. 2010.

[19] Chrystal, P., McKnight, D., Meredith, P. L., Schmidt, J., Fok, M., and Wetton, C., "Space Debris: On Collision Course for Insurers?" Tech. Rept. 1504360-11-en, Swiss Reinsurance Company Ltd., Zurich, March 2011.

[20] Oltrogge, D. L., Alfano, S., Law, C., Cacioni, A., and Kelso, T. S., "A Comprehensive Assessment of Collision Likelihood in Geosynchronous Earth Orbit," *Acta Astronautica*, Vol. 147, June 2018, pp. 316–345.

[21] Schaub, H., and Sternovsky, Z., "Active Space Debris Charging for Contactless Electrostatic Disposal Maneuvers," *Advances in Space Research*, Vol. 53, No. 1, Jan. 2014, pp. 110–118. https://doi.org/10.1016/j.asr.2013.10.003

[22] Hogan, E. A., and Schaub, H., "Impacts of Hot Space Plasma and Ion Beam Emission on Electrostatic Tractor Performance," *IEEE Transactions on Plasma Science*, Vol. 43, No. 9, 2015, pp. 3115–3129. https://doi.org/10.1109/TPS.2015.2451001

[23] Hogan, E., and Schaub, H., "Space Weather Influence on Relative Motion Control Using the Touchless Electrostatic Tractor," *Journal of Astronautical Sciences*, Vol. 63, No. 3, 2016, pp. 237–262. https://doi.org/10.1007/s40295-016-0090-4

[24] Denton, M. H., Thomsen, M. F., Korth, H., Lynch, S., Zhang, J. C., and Liemohn, M. W., "Bulk Plasma Properties at Geosynchronous Orbit," *Journal of Geophysical Research*, Vol. 110, No. A7, July 2005. https://doi.org/10.1029/2004JA010861

[25] Hughes, J., and Schaub, H., "Prospects of Using a Pulsed Electrostatic Tractor with Nominal Geosynchronous Conditions," *IEEE Transactions on Plasma Science*, Vol. 45, No. 8, 2017, pp. 1887–1897. https://doi.org/10.1109/TPS.2017.2684621

[26] Hughes, J., and Schaub, H., "Orbital and Storm Time Analysis of the Pulsed Electrostatic Tractor," *European Conference on Space Debris*, European Space Operations Centre, Darmstadt, Germany, April 2017.

[27] Denton, M., Thompsen, M., Jordanova, V., Henderson, M., Borovsky, J., Denton, J., Pitchford, D., and Hartley, D., "An Empirical Model of Electron and Ion Fluxes Derived from Observations at Geosynchronous Orbit," *AGU Space Weather*, Vol. 13, No. 4, 2015, pp. 233–249. https://doi.org/10.1002/2015SW001168

[28] Davis, V., Gardner, B., Mandell, M., and Wilcox, K., *NASCAP-2k User's Manual*, 4th ed., Science Applications International Corp., San Diego, CA, Feb. 2011, p. 26.

[29] Borovsky, J. E., Cayton, T. E., Denton, M. H., Belian, R. D., Christensen, R. A., and Ingraham, J. C., "The Proton and Electron Radiation Belts at Geosynchronous Orbit: Statistics and Behavior During High-Speed Stream-Driven Storms," *Journal of Geophysical Research: Space Physics*, Vol. 121, No. 6, June 2016, pp. 5449–5488. https://doi.org/10.1002/2016JA022520

[30] Hughes, J., and Schaub, H., "Space Weather Influence on Electromagnetic Geosynchronous Debris Perturbations Using Statistical Fluxes," *Space Weather*, Vol. 16, No. 4, 2018, pp. 391–405.

[31] Davis, V., and Mandell, M. J., *Plasma Interactions with Spacecraft*, 4th ed., Vol. 2, NASCAP-2K Scientific Documentation for Ver. 4.1, Science Applications International Corp., 2011.

[32] Davis, V. A., Mandell, M. J., and Thomsen, M. F., "Representation of the Measured Geosynchronous Plasma Environment in Spacecraft Charging Calculations," *Journal of Geophysical Research*, Vol. 113, No. A10, 2008. https://doi.org/10.1029/2008JA013116

[33] Katz, I., Parks, D. E., Mandell, M., Harvey, J. M., Brownell, D. H., Wang, S., and Rotenberg, M., "A Three Dimensional Dynamic Study of Electrostatic Charging in Materials," Tech. Rept., Systems, Science, and Software, 1977, https://ntrs.nasa.gov/archive/nasa/casi.ntrs.nasa.gov/19780005385.pdf.

[34] Ferguson, D., Hilmer, R., and Davis, V., "Best Geosyncronous Earth Orbit Daytime Scpacecraft Charging Index," *Journal of Spacecraft and Rockets*, Vol. 52, No. 2, 2015, pp. 526–543. https://doi.org/10.2514/1.A32959

[35] Lai, S. T., *Fundamentals of Spacecraft Charging: Spacecraft Interactions with Space Plasmas*, Princeton Univ. Press, Princeton, NJ, 2011.
[36] Gussenhoven, M., Mullen, E., and Hardy, D., "Artificial Charging of Spacecraft Due to Electron Beam Emission," *IEEE Transactions on Nuclear Science*, Vol. 34, No. 6, 1987, pp. 1614–1619.
[37] Schnueller, G. W., Mandell, M. J., Parks, D. E., Steen, P. G., Cassidey, J. J., Katz, I., and Rubin, A., "Charging Analysis of the SCATHA Satellite," Tech. Rept. NAS3-21050, Air Force Geophysics Lab., 1979.
[38] Seubert, C. R., Stiles, L. A., and Schaub, H., "Effective Coulomb Force Modeling for Spacecraft in Earth Orbit Plasmas," *Advances in Space Research*, Vol. 54, No. 2, 2014, pp. 209–220.
[39] Garrett, H. B., "Review of Quantitative Models of the 0 to 1 keV Near-Earth Plasma," *Reviews of Geophysics and Space Physics*, Vol. 17, No. 3, May 1979, pp. 397–417. https://doi.org/10.1029/RG017i003p00397
[40] Hogan, E. A., "Impacts of Tug and Debris Sizes on Electrostatic Tractor Charging Performance," *Advances in Space Research*, Vol. 55, No. 2, Jan. 2015, pp. 630–638. https://doi.org/10.1016/j.asr.2014.10.023

J. Reuther
Associate Editor